The Zeeman Effect in Mercury and Neon

William Bidle and Beatrice Liang-Gilman
Department of Physics and Astronomy, Rutgers University
(Dated: 10 December 2020)

Abstract In this report, we study the Zeeman fine structure of mercury and neon through high resolution spectroscopy using a Czerny-Turner scanning spectrometer. We use the 546.1 nm green line, 435.8 nm blue line, and 404.7 nm violet line of mercury, as well as the 585.3 nm green line of neon, each in magnetic fields of up to $1.5\,T$. By comparing our measurements against the theoretical values of g_{eff}, we determine the electron charge to mass ratio, $^{e}/_{m}$, to be as good as $(1.68 \pm 0.05) \times 10^{11}\,\frac{C}{kg}$, which is in agreement with the widely accepted value of $1.76 \times 10^{11}\,\frac{C}{kg}$. In addition, we also present a study of the Hydrogen Balmer lines compared with theoretical expectations.

I. INTRODUCTION AND THEORY

The broadening of atomic energy levels in the presence of an external magnetic field was first observed by Pieter Zeeman in 1896, 10 years before the invention of quantum mechanics. By measuring the spectral line broadening of a sodium discharge tube in a magnetic field, Zeeman was able to determine the charge to mass ratio, $^{e}/_{m}$, of electron. The following theoretical discussion is a simplified version of the ones presented in [1] and [2].

I.1. The Zeeman Effect

An electron of mass m_e and charge e orbiting a nucleus produces a magnetic dipole moment $\vec{\mu}$, which is proportional to its angular momentum $\vec{L}$. If an external magnetic field B is applied to the system, it will induce a shift in the electron's orbital energy levels:

$$\Delta E = -\vec{\mu} \cdot \vec{B} = -\frac{e}{2m_e} L_z B \qquad (1)$$

Extending this relation to quantum theory, an electron with angular momentum quantum number l, magnetic quantum number $m = -l, -l+1, \ldots l$, and angular momentum along the direction of the magnetic field $L_z = m\hbar$, has its energy levels shifted by:

$$\Delta E_m = -\frac{e}{2m_e} m\hbar B = \mu_B m B \qquad (2)$$

Where μ_B is the Bohr magneton. This results in each nl energy level splitting into $2l+1$ sub-levels with equal spacing of $\mu_B B$. This effect results in spectral line broadening of a gas in a discharge tube, where electrons make electron-dipole transitions from an initial state to a lower energy state. In this transition, a photon is released which carries away the difference in energy between the two states. Since photons always carry an angular momentum of $\hbar$, this also limits the allowed electron transitions to occur between states where $\Delta l = \pm 1$ and $\Delta m = 0, \pm 1$. Therefore, regardless of the l values involved in a given transition, only three lines are produced.

I.2. The Anomalous Zeeman Effect

In practice, however, this normal three-line Zeeman effect is not observed. What is commonly found is that the applied magnetic field splits the energy levels into more than three lines. This effect can be understood due to the presence of the electron's spin, $\vec{S}$, contributing to its dipole moment. As a result, the total magnetic moment of an electron is given by:

$$\vec{\mu} = \frac{e}{2m_e}\left(g * \vec{S} + \vec{L}\right) = \frac{e}{2m_e}\left(\vec{J} + \vec{S}\right) \qquad (3)$$

Where g is the g-factor of the electron, taken here to be 2, and the last step uses the relationship $\vec{J} = \vec{L} + \vec{S}$.[1] The resulting shift in the electron's energy states is then:

$$\Delta E = -\frac{e}{2m_e}\left(\vec{J} + \vec{S}\right) \cdot \vec{B} = -g_L \mu_B m_j B \qquad (4)$$

Where g_L is the Landé g-factor, determined through operator algebra [2]. For an electron with angular momenta numbers l, s, and j, the Landé g-factor can be found as:

$$g = 1 + \frac{j(j+1) + s(s+1) - l(l+1)}{2j(j+1)} \qquad (5)$$

[1] The real value of g is closer to 2.0023, however for the purposes of this report it is good enough to approximate to 2.

If the transition takes place between levels with the same m_j, then the photon's energy is unshifted by the applied magnetic field. However, if the change in m_j is ± 1 between levels, then the shift in photon energy is given by:

$$\Delta E = \left(m_j g_L - m_j{}' g_L{}'\right)\mu_B B = g_{eff}\mu_B B \qquad (6)$$

Where g_{eff} is the effective g-factor for the transition. Note that the normal three-line Zeeman effect will appear if $g_L = g_L{}'$, otherwise there will be more than three lines, resulting in the so-called anomalous Zeeman effect.

I.3. Zeeman Effect in Mercury

The Zeeman effect is more complicated for atoms with several electrons, however, since full shells and subshells have zero contributions to the overall state, the net $\vec{S}$, $\vec{L}$, and $\vec{J}$ are due solely to the presence of the valence electrons. In the example of mercury, a single atom contains 80 electrons, and the ground state is $^1S_0$ in LS notation. The first excited levels above the ground state in mercury are the triplet levels, $^3P_0$, $^3P_1$, and $^3P_2$, which will be studied in this experiment.

Only specific transitions are allowed between Zeeman shifted states. These allowed transitions form σ lines when photons are emitted in a transition where Δm_j = ±1, and π lines when Δm_j = 0. σ lines can only be observed when polarized perpendicular to the magnetic field, and π lines need to be polarized parallel to the magnetic field to be seen. The theoretical Zeeman splitting of the 404.7 nm violet line, 435.8 nm blue line, and 546.1 nm green line can be seen in Figure 1, Figure 2, and Figure 3 respectively.

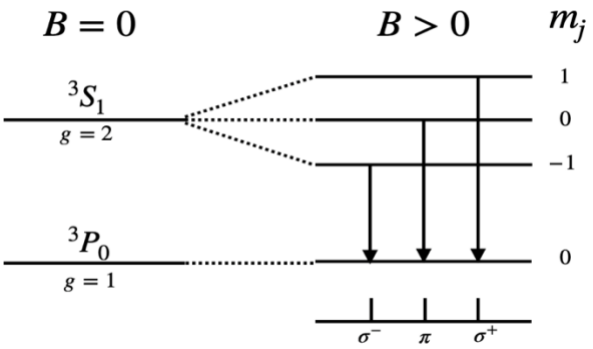

Figure 1: Energy level diagram for the 404.7 nm violet line of mercury, due to the $^3S_1 \rightarrow {}^3P_0$ transition.

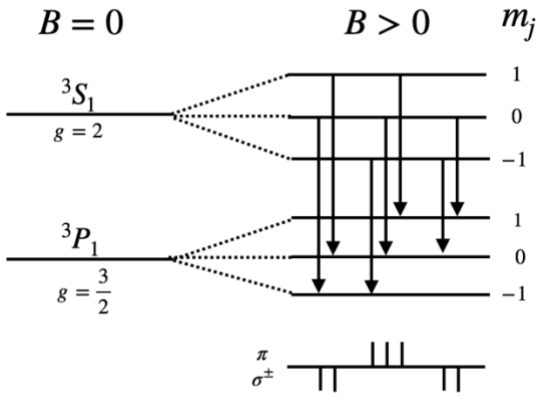

Figure 2: Energy level diagram for the 435.8 nm blue line of mercury, due to the $^3S_1 \rightarrow {}^3P_1$ transition.

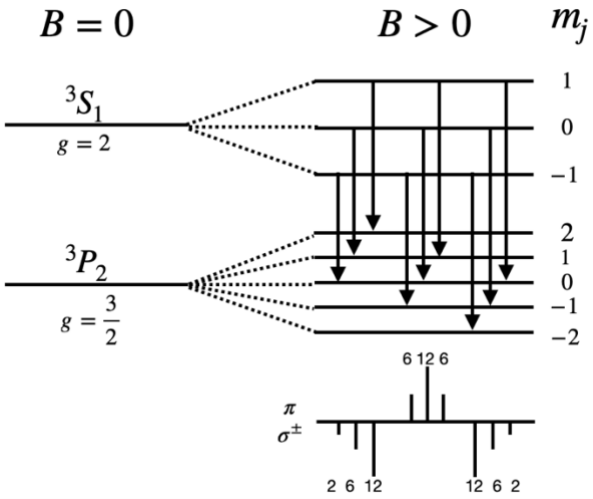

Figure 3: Energy level diagram for the 546.1 nm green line of mercury, due to the $^3S_1 \rightarrow {}^3P_2$ transition. The numbers above the σ and π lines represent the relative strengths of each transition.

I.4. Zeeman Effect in Neon

Neon contains 10 electrons which completely fill the $n = 1$ and $n = 2$ shells, leaving $\vec{S} = \vec{L} = \vec{J} = 0$ and an LS notation of $^1S_0$. The strong orange line at 585.3 nm that will be studied in this report is caused by an excited electron in a $3P$ level moving to a $3S$ level, which corresponds to the transition $^1S_0 \rightarrow {}^1P_1$ in LS notation. Since both initial and final states are close to pure states, the LS coupling that was assumed in the derivation of the Landé g-factor is a good enough approximation for this study. The theoretical Zeeman splitting of the 585.3 nm orange line can be seen in Figure 4.

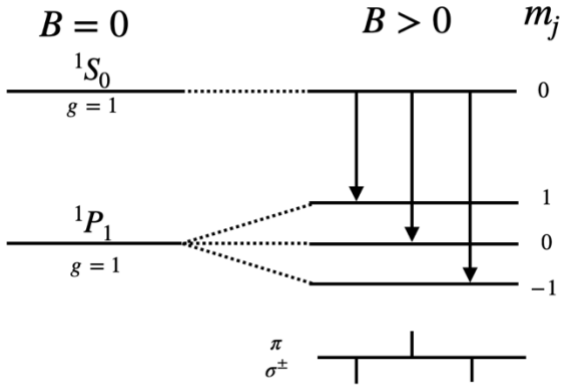

Figure 4: Energy level diagram for the 585.3 nm orange line of neon, due to the $^1S_0 \rightarrow {}^1P_1$ transition.

I.5. Balmer Transitions in Hydrogen

Spectral emission occurs when an electron in a higher energy state jumps to a lower energy state and emits a photon. The series of transitions where this final state is the energy state with quantum number $n = 2$ is known as the Balmer series. The hydrogen Balmer series is notable because the first four transitions of the series emit photons that appear with wavelengths in the spectrum of visible light. Any atomic electron transition can be described using the Rydberg formula, where λ is the wavelength of the emitted photon, Z is the atomic number, n_i is the initial energy level, n_f is the final energy level, and R_H is the Rydberg constant.

$$\frac{1}{\lambda} = R_H\left(\frac{1}{n_i^2} - \frac{1}{n_f^2}\right) \qquad (7)$$

II. APPARATUS AND PROCEDURE

II.1. The Czerny-Turner Spectrometer

The apparatus used in the experiment is a Spex 1000M Czerny-Turner scanning spectrometer, which can be seen in Figure 5. The device uses a holographic diffraction grating with 1800 grooves/cm to disperse the measured light by wavelength into a spectrum. The spectrum is scanned by rotating the grating to capture light of a particular wavelength onto the detector. The size of the entrance and exit slits can be increased to allow for more light to reach the detector, but also decreased to improve the resolution. The entire apparatus is controlled remotely from the laboratory computer, allowing for an adjustable step size (e.g., 0.005 nm/step) and integration time (e.g., 0.1 s/step).

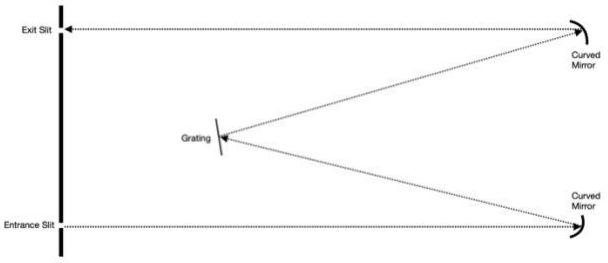

Figure 5: A schematic of Spex 1000M Czerny-Turner Scanning Spectrometer

A small enough spectrometer resolution is necessary to see each of the lines of the Zeeman splitting. The instrument resolution used in this experiment is set to 0.006 nm. This resolution value is determined by the full width of the spectral line at half its full intensity. In order for a well resolved spectrum to be seen, the linewidth of the instrument must be smaller than the Zeeman splitting:

$$|\Delta\lambda| = g_{eff}\frac{\lambda^2}{hc}\mu_B B \qquad (8)$$

Otherwise, a peak broadening occurs, disguising multiple peaks as one line. In this experiment the resolution is only slightly smaller than the Zeeman splitting of each line studied. For example, the 435.8 nm line yields $|\Delta\lambda| \approx 0.009$ nm, which means that the resolution isn't small enough to clearly resolve the individual peaks. Simulation plots are later included to see how a smaller instrument resolution would affect the resolution of individual peaks that can be seen for each wavelength. These plots were made using a summation of Lorentzian functions:

$$I(\lambda) = \frac{1}{\pi\delta\lambda} * \frac{1}{1+\frac{(\lambda-\lambda_0)^2}{(\delta\lambda)^2}} \qquad (9)$$

Where λ is the wavelength, λ_0 is the center of the peak, and $\delta\lambda$ is the half-width caused by instrument resolution. In addition to studying the effect of instrument resolution, we examined the effect of the Doppler broadening on the natural linewidth. We found that the largest Doppler broadening came from the 546.8 nm line. Assuming a working temperature of 500K, the distribution of velocities in the gas cause the Doppler broadening to be approximately 0.0006 nm. As this is smaller than the instrument resolution of 0.006 nm by a factor of 10, we determined this effect to be negligible for the experiment.

II.2. Zeeman Splitting Predictions

Before starting the experiment, the predicted Zeeman splitting for the three mercury lines and the neon orange line were calculated. A linear polarizer was used to filter out the two different types of transitions, corresponding to the so-called π and σ lines. Transitions with $\Delta m = 0$ are labeled π

lines and can be observed when the polaroid filter is aligned parallel to the magnetic field. Conversely, transitions with $\Delta m = \pm 1$ are labeled σ lines and can be seen when the polaroid filter is aligned perpendicular to the magnetic field. The values for g_{eff} were calculated using the equations detailed in section I.2, and can be seen in Table 1 - Table 4 below. For each situation, m_j' corresponds to the magnetic quantum numbers of the $^3S_1$ state, and m_j corresponds to the magnetic quantum numbers of the ^3P states.

Allowed Transitions of $^3S_1 \rightarrow {}^3P_0$ in Mercury				
m_j'	m_j	Δm	polarization	$g_{eff} = m_j - 2m_j'$
-1	0	1	σ	2
0	0	0	π	0
1	0	-1	σ	-2

Table 1: Table of theoretically allowed transitions for Zeeman splitting of $^3S_1 \rightarrow {}^3P_0$.

Allowed Transitions of $^3S_1 \rightarrow {}^3P_1$ in Mercury				
m_j'	m_j	Δm	polarization	$g_{eff} = \frac{3}{2}m_j - 2m_j'$
-1	0	1	σ	2
0	1	1	σ	3/2
-1	-1	0	π	1/2
0	0	0	π	0
1	1	0	π	-1/2
0	-1	-1	σ	-3/2
1	0	-1	σ	-2

Table 2: Table of theoretically allowed transitions for Zeeman splitting of $^3S_1 \rightarrow {}^3P_1$.

Allowed Transitions of $^3S_1 \rightarrow {}^3P_2$ in Mercury				
m_j'	m_j	Δm	polarization	$g_{eff} = \frac{3}{2}m_j - 2m_j'$
-1	0	1	σ	2
0	1	1	σ	3/2
1	2	1	σ	1
-1	-1	0	π	1/2
0	0	0	π	0
1	1	0	π	-1/2
-1	-2	-1	σ	-1
0	-1	-1	σ	-3/2
1	0	-1	σ	-2

Table 3: Table of theoretically allowed transitions for Zeeman splitting of $^3S_1 \rightarrow {}^3P_2$.

Allowed Transitions of $^1S_0 \rightarrow {}^1P_1$ in Neon				
m_j'	m_j	Δm	polarization	$g_{eff} = m_j - m_j'$
0	1	1	σ	1
0	0	0	π	0
0	-1	-1	σ	-1

Table 4: Table of theoretically allowed transitions for Zeeman splitting of $^1S_0 \rightarrow {}^1P_1$. This transition behaves just like the "normal" Zeeman effect.

II.3. Experimental Procedure

Before collecting data, it was necessary to establish the hysteresis curve for the electromagnet used throughout the experiment. This is an important process as it helps to prevent lag between the set current and the produced magnetic field. To do this, the current in the magnet was raised to 9 amperes, then lowered back to 0 amperes. The magnet was then turned off, the polarity was switched, and the current was raised to 8 amperes and then lowered back to 0 amperes. This process of switching the polarity and lowering the current was continued until the current reached ½ an ampere. Throughout the experiment, it was important to ensure that each time the current needed to be raised or the magnet needed to be turned off, the current was first decreased back to 0.

Once the magnet and computer system were ready for data collection, the mercury discharge tube was placed and centered in the magnet gap. With the magnet off, a few scans were performed to determine the best range of wavelengths, integration times, and step sizes needed to clearly resolve the 404.7 nm mercury line. The magnet was then turned up to 10 amperes, and optimal angular positions of the polaroid filter were determined to be used throughout the experiment. We found that values of 110° and 20° gave the best results for the π and σ spectra, respectively. In addition to taking scans for the σ and π lines with the current at 10 amperes, the σ lines were measured at other current values to get a range of data points to calculate g_{eff}. The scans were all taken with an integration time of 0.03 seconds. At each point that the current for the magnetic field was adjusted, a Hall probe was used to measure the magnetic field value. The Zeeman splitting was plotted as a function of the applied magnetic field, where the slope of the linear fit was used to find g_{eff}. We determined g_{eff} to be half the value of the slope, since we were plotting the distance between peaks, rather than the distance of each peak from the center π line.

A similar procedure was used to find g_{eff} for the mercury 435.8 nm and 546.1 nm lines. The π line was measured at 10 amperes, and the σ lines were measured at a range of magnetic field values. The σ spectra splitting values were again plotted as a function of magnetic field, and the slope was extracted to find g_{eff}. For these two lines, it is important to note that the resolution of the spectrometer is not high enough to see each individual σ or π line. Thus, only one peak is seen where two or three lines actually exist. While the anomalous Zeeman effect is not directly seen, its effect can be observed in the resulting g_{eff} values.

Finally, the mercury sample was then replaced with a neon discharge tube in order to study the 585.3 nm line of the neon spectrum. This time, the π line was measured at 5 amperes, and the σ lines were measured at a range of magnetic field values around 5 amps. Again, the Zeeman splitting was plotted as a function of the magnetic field to find g_{eff} for this line.

II.4. Electron Charge to Mass Ratio

The charge to mass ratio can be easily extracted from the Zeeman effect. Given g_{eff}, the magnetic field, and the Zeeman splitting, all the components are available to find the charge to mass ratio of the electron. By rearranging Equation 6, and using the definition of μ_B from Equation 2, the charge to mass ratio $\frac{e}{m}$ can be represented as the slope of a linear equation:

$$\frac{4\pi\Delta\nu}{g_{eff}} = B * \frac{e}{m} \qquad (10)$$

For this part of the experiment, we used the given g_{eff} and values for Zeeman splitting that we extracted from data, and the values for magnetic field found using the Hall probe. Once all the data points were plotted, we drew a line of best fit through them, and compared the slope to the accepted value of the electron charge to mass ratio.

II.5. The Balmer Lines of Hydrogen

In addition to studying Zeeman splitting in mercury and neon, we analyzed the first few Balmer transitions in Hydrogen to compare with theoretical predictions. The predicted wavelengths were calculated using the Rydberg formula described above. The theoretical values can be seen in Table 5.

n_i	n_f	Wavelength (nm) (calculated)
3	2	656.47
4	2	486.28
5	2	434.18
6	2	410.30
7	2	397.13
8	2	389.02

Table 5: Calculated theoretical values for wavelengths of hydrogen Balmer lines.

II.6. Errors

To account for error, we first included a ± 0.03 T error for each of our magnetic field values. This was determined by deviation in the displayed values on the Hall probe, and to account for imprecise positioning of the probe between the magnet. In addition, we incorporated error in the intensity from the data. The values for intensity are proportional to the number of counts per second at each wavelength, which we calculated by using:

$$\delta I = \frac{\sqrt{n*t}}{t} \qquad (11)$$

Where n is the counts per second, and t is the integration time. This was necessary to get the raw counts the machine took, to find the standard error of the sample.

III. DATA AND ANALYSIS

III.1. Mercury $^3S_1 \rightarrow {}^3P_0$ Transition

The Zeeman effect in the 404.7 nm mercury line was recorded at various magnetic field values, and the resulting can be seen in Figure 6. The individual spectra can be seen in the Appendix along with their fits.

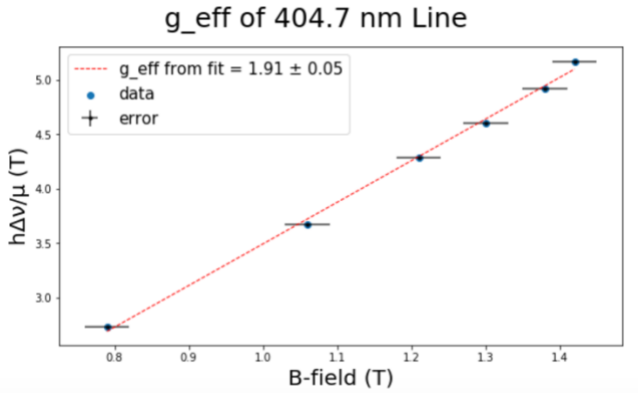

Figure 6: Zeeman splitting as a function of the magnetic field for the mercury 404.7 nm line.

From the fit, it can be seen that the g_{eff} was found to be 1.91 ± 0.05, which is in good agreement with the expected value of $g_{eff} = 2$. The 404.7 nm line has the simplest splitting of the three measured mercury lines for this experiment, with only two σ lines and one π line.

III.2. Mercury $^3S_1 \rightarrow {}^3P_1$ Transition

The Zeeman splitting of the mercury 435.8 nm line was recorded various magnetic field values in order to determine g_{eff}. This splitting was calculated in a similar manner as before and can be seen plotted against the magnetic field below. The individual spectra can be seen in the Appendix along with their fits.

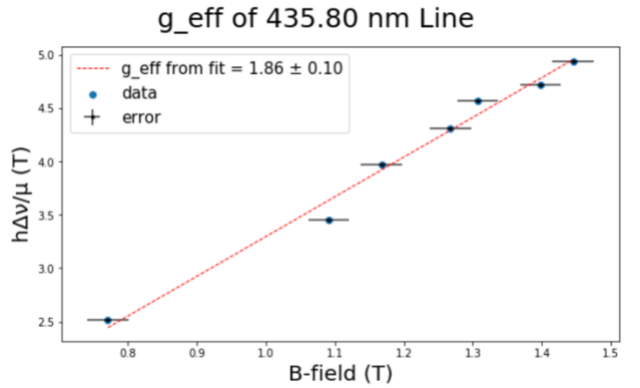

Figure 7: Zeeman splitting as a function of the magnetic field for the mercury 435.8 nm line.

For the mercury 435.8 nm line, although only two σ peaks can be seen in each scan the instrument took (see the Appendix), each of those peaks actually contains two σ peaks each, which is exactly what we expect theoretically (see Figure 2). According to Table 2, the σ peaks should show up at ±1.5 and ±2 with equal intensities, so we expect the peak broadening to cause g_{eff} to be around 1.75, the average of the individual peak splitting. The slope of the fit on the collected Zeeman splitting data gives a $g_{eff} = 1.86 \pm 0.10$ This value is close to the expected $g_{eff} = 1.75$.

As discussed in II.1, the individual σ peaks cannot be directly seen due to the instrument resolution not being small enough. To look at this more closely, the simulation in Figure 8 depicts the spectra at instrument resolutions of 0.06 Å, 0.03 Å, and 0.012 Å. As seen, a resolution of around 0.012 Å allows for a clear resolution of the individual σ peaks.

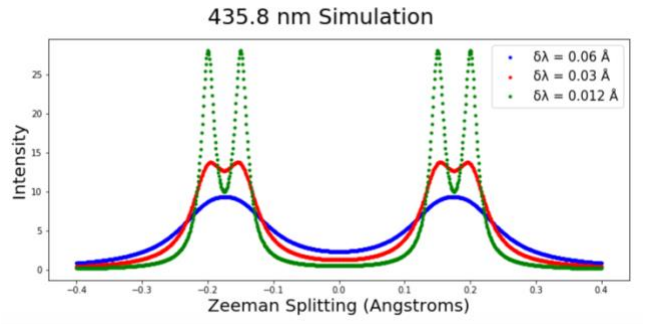

Figure 8: Simulation of mercury 435.8 nm line transition at different resolutions.

III.3. Mercury $^3S_1 \rightarrow {}^3P_2$ Transition

The $^3S_1$ to $^3P_2$ transition again uses various magnetic field values to draw a fit through the plot of Zeeman splitting as a function of magnetic field. The individual spectra can be seen in the Appendix along with their fits.

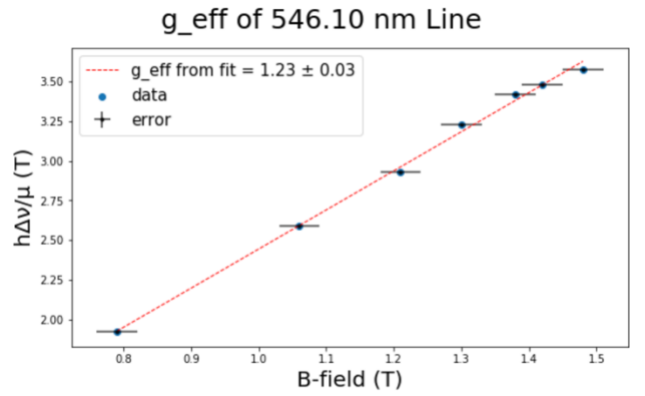

Figure 9: Zeeman splitting as a function of the magnetic field for the mercury 546.1 nm line.

The 546.1 nm mercury line produces six σ lines which are resolved into two peaks in our data. These six lines split with values of ±1, ±1.5, and ±2, so we originally expected g_{eff} to be about 1.5. However, these transitions actually occur at different strengths, as depicted in Figure 3, shifting the expected value of g_{eff} to be 1.25. As can be seen in Figure 9 above, the extracted value of $g_{eff} = 1.23 \pm 0.03$, which is within error of the expected value of 1.25.

Again, an analysis of the effect of different instrument resolutions is done below. The simulation below shows how a resolution of about 0.003 Å is needed to effectively show all six sigma peaks and their varying strengths. It can also be seen, however, that the overall shape of the lower resolution captures the behavior of the split peaks. Because of this, even at lower resolutions, such as the one used in the experiment, an accurate determination of g_{eff} can be achieved.

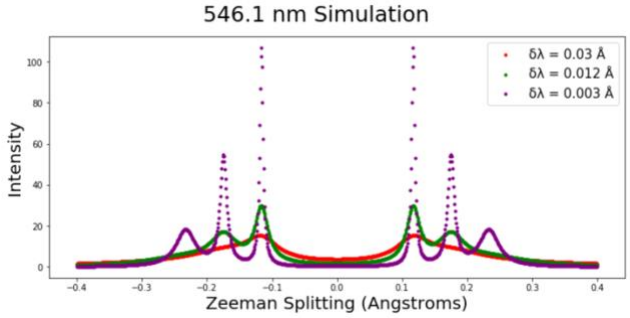

Figure 10: Simulation of mercury 546.1 nm line transition at different resolutions.

III.4. Neon $^1S_0 \rightarrow {}^1P_1$ Transition

The same analysis that was used for the mercury lines was performed on the neon $^1S_0 \rightarrow {}^1P_1$ transition. The plot of Zeeman splitting as a function of magnetic field can be seen below.

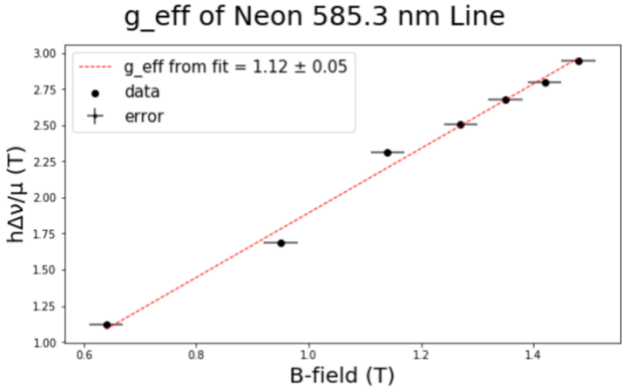

Figure 11: Zeeman splitting as a function of the magnetic field for the neon 585.3 nm line.

The fit on the neon data produces a $g_{eff} = 1.12 \pm 0.05$, which is similar to the predicted value of $g_{eff} = 1$. This line does not require a smaller resolution, as there are only two σ peaks, which are split at ±1. In addition, the g-factors of both the initial and final states of this transition are 1.

III.5. Calculation of $^{e}/_{m}$

The accepted value for the charge to mass ratio of the electron is $1.76 \times 10^{11} \frac{C}{kg}$. Below are the plots used to extract the charge to mass ratio using our data of the mercury 404.7 nm and 435.8 nm lines.

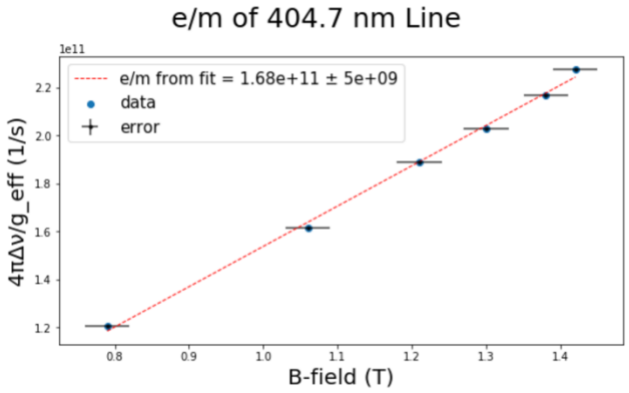

Figure 12: Charge to mass ratio extraction using linear fit on the mercury 404.7 nm line.

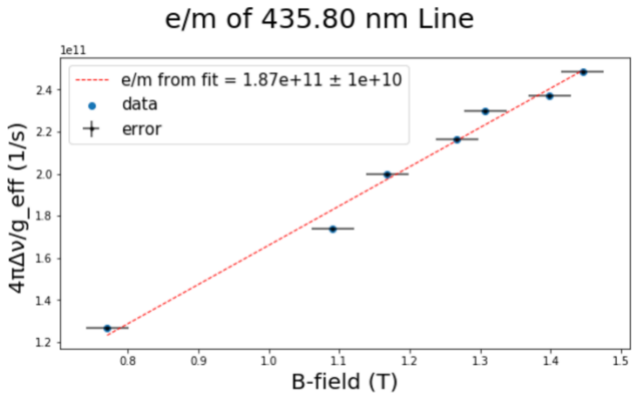

Figure 13: Charge to mass ratio extraction using linear fit on the mercury 435.8 nm line.

The value extracted from the fit for the 404.7 nm mercury line shown above is $(1.68 \pm 0.05) \times 10^{11} \frac{C}{kg}$, while the extracted value from the fit of the 435.8 nm line is $(1.87 \pm 0.10) \times 10^{11} \frac{C}{kg}$. Both of these calculated values are in good agreement with the accepted value of the charge to mass ratio.

III.6. Hydrogen Balmer Lines

Using the predicted values from Table 5 for where the Balmer series transitions will appear, data was taken at the corresponding wavelengths. As can be seen in Table 6, the experimentally determined wavelengths appear very close to the accepted values.

n_i	n_f	Wavelength (nm) (from fit)	Wavelength (nm) (theoretical)	Difference
3	2	656.77	656.47	0.298
4	2	486.62	486.28	0.347
5	2	434.53	434.18	0.355
6	2	410.65	410.30	0.354
7	2	397.47	397.13	0.344

Table 6: Difference between experimentally determined and accepted values of Balmer transition wavelengths.

IV. CONCLUSION

By using a high-resolution Czerny-Turner scanning spectrometer, we were able to effectively observe the Zeeman structure of mercury and neon discharge tubes when they were placed in an external magnetic field. While the anomalous Zeeman effect was difficult to directly observe, its effects could be measured when calculating the effective splitting of each line.

Based off of our measurements of the mercury 404.7 nm line and 435.8 nm line, we determined the charge to mass ratio of the electron to be $(1.68 \pm 0.05) \times 10^{11} \frac{C}{kg}$ and $(1.87 \pm 0.10) \times 10^{11} \frac{C}{kg}$, respectively. These values are within about 5% of the accepted value of $1.76 \times 10^{11} \frac{C}{kg}$.

V. REFERENECES

[1] D. J. Griffiths, *Introduction to Quantum Mechanics* (Cambridge University Press, 2018).

[2] A. Melissinos, *Experiments in Modern Physics* (Academic Press, 2003).

VI. APPENDIX

Displayed below are the individual plots of the data gathered throughout the experiment used in the calculation of g_{eff} for each line. Each set of data was fit with Lorentzian functions to capture the overall profile of the Zeeman splitting used in the calculation of g_{eff} and the charge to mass ratio of the electron.

VI.1. Mercury $^3S_1 \rightarrow {}^3P_0$ Transition

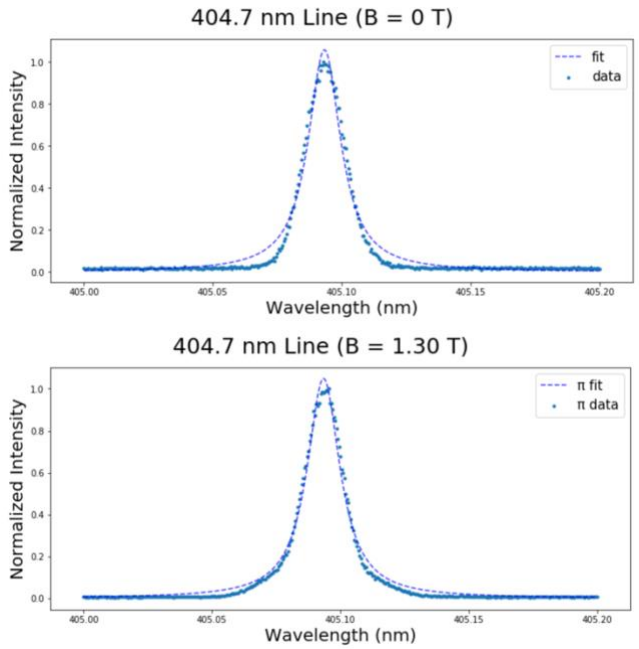

Figure 14 (a-b): Raw data with Lorentzian fit of mercury 404.7 nm π line at different magnetic field values.

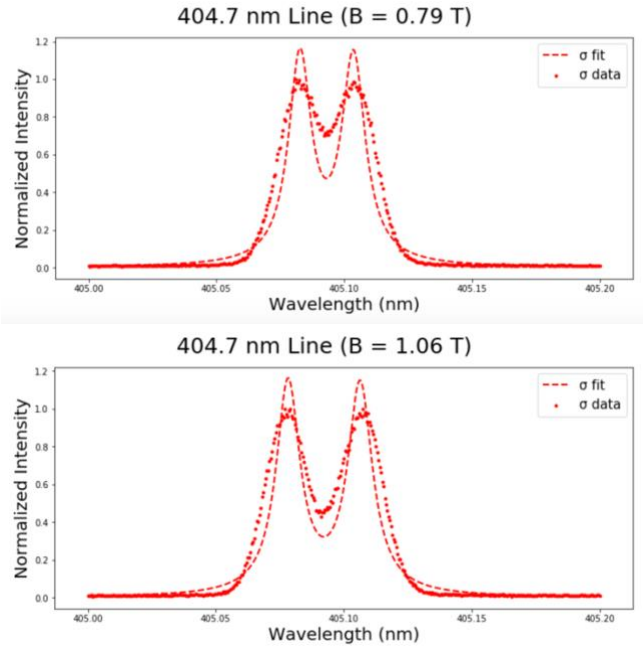

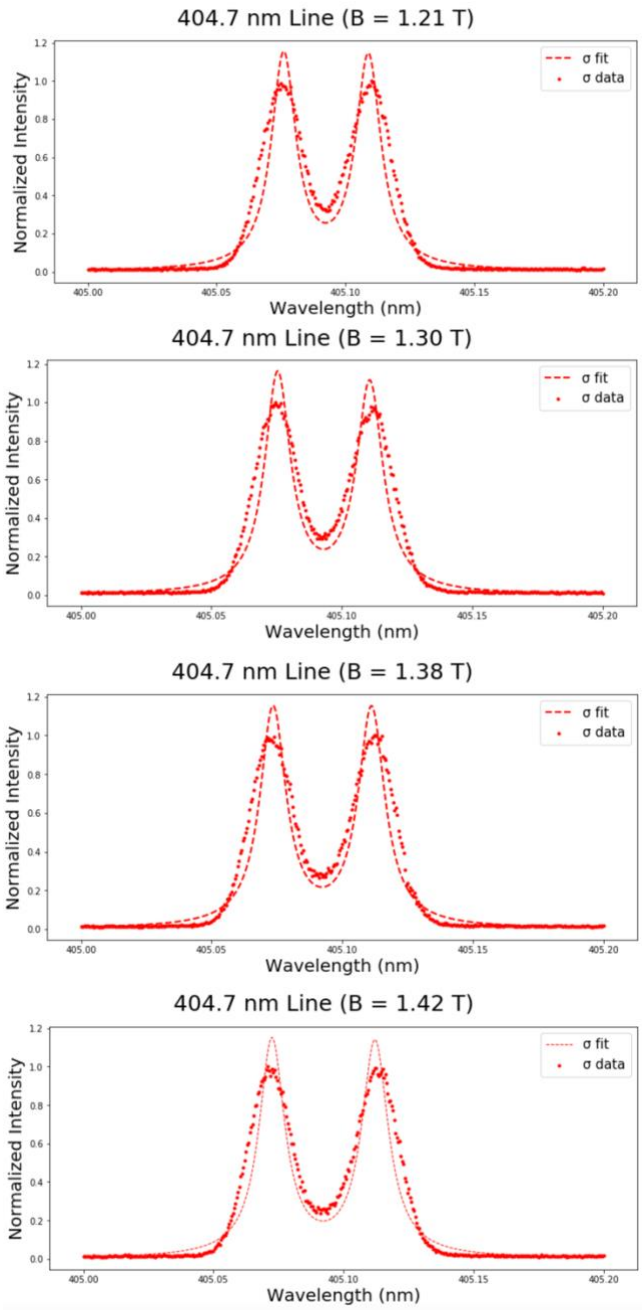

Figure 15 (a-f): Raw data with Lorentzian fits of mercury 404.7 nm σ lines at different magnetic field values.

VI.2. Mercury $^3S_1 \rightarrow {}^3P_1$ Transition

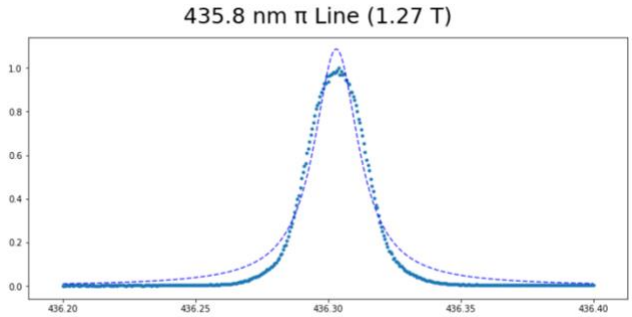

Figure 16: Raw data with Lorentzian fit of mercury 435.8 nm π line.

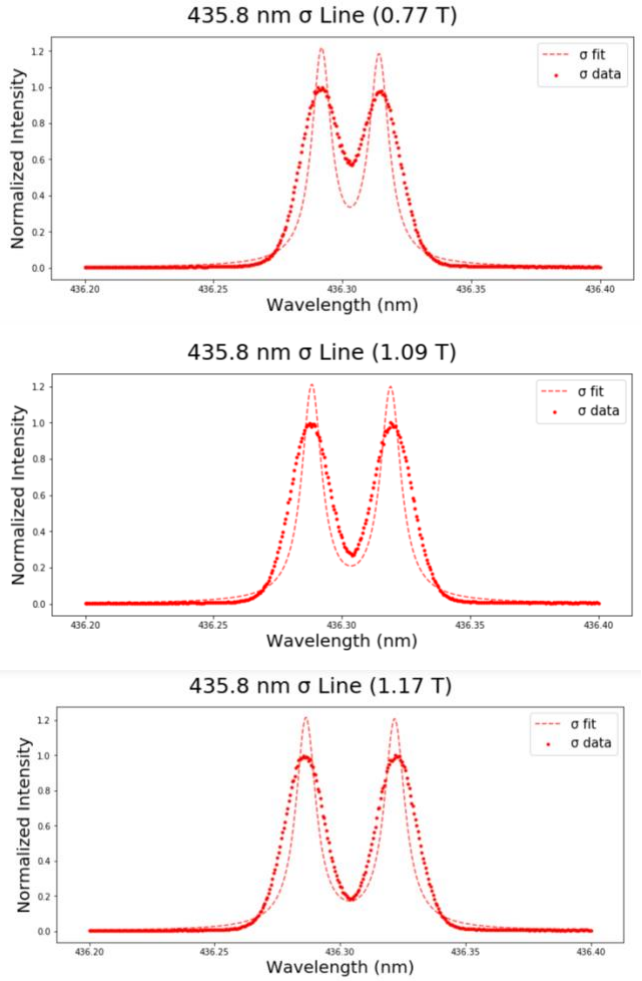

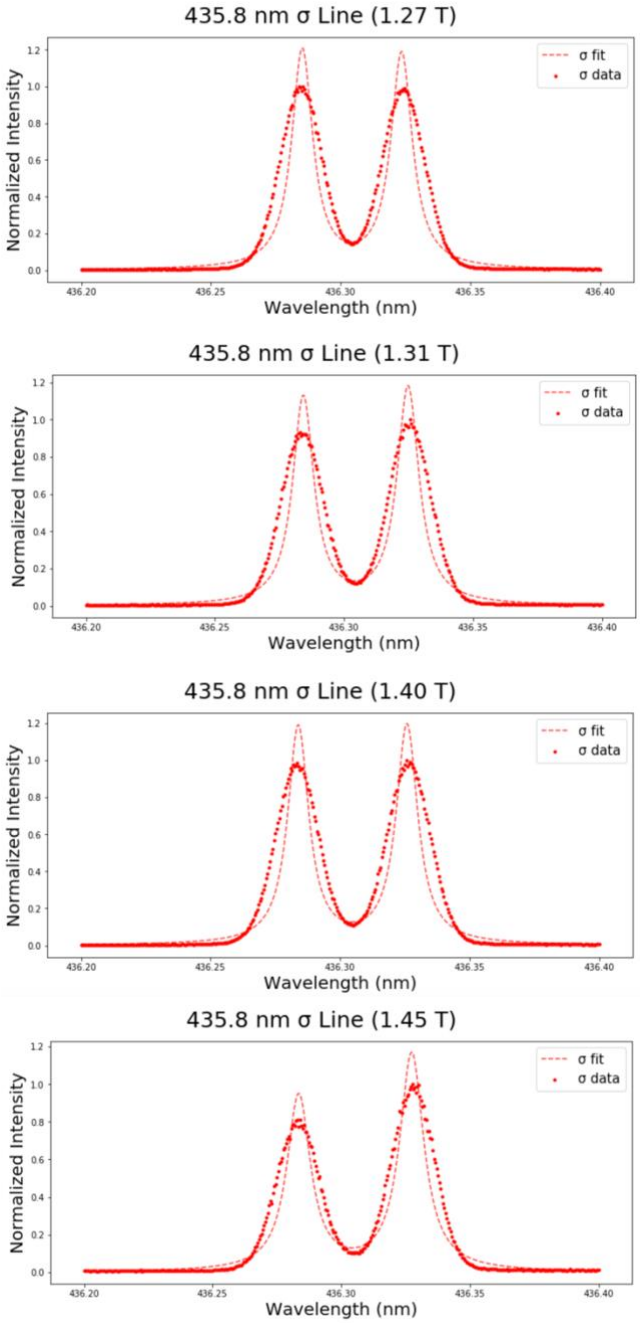

Figure 17 (a-g): Raw data with Lorentzian fits of mercury 435.8 nm σ lines at different magnetic field values.

VI.3. Mercury $^3S_1 \rightarrow {}^3P_2$ Transition

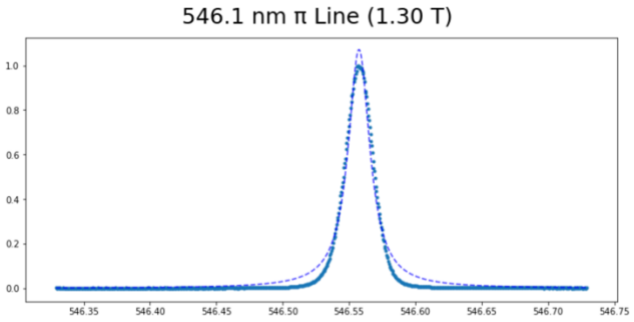

Figure 18: Raw data with Lorentzian fit of mercury 546.1 nm π line.

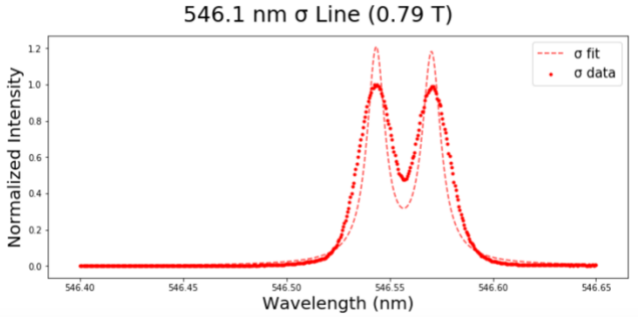

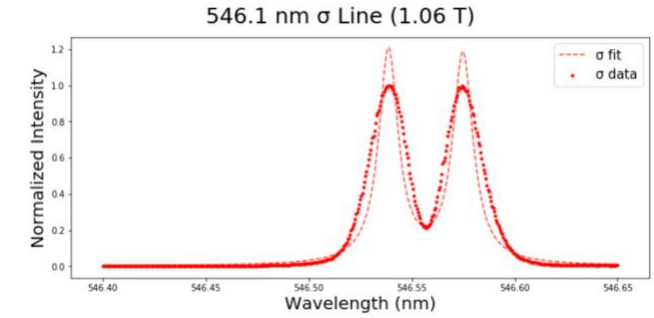

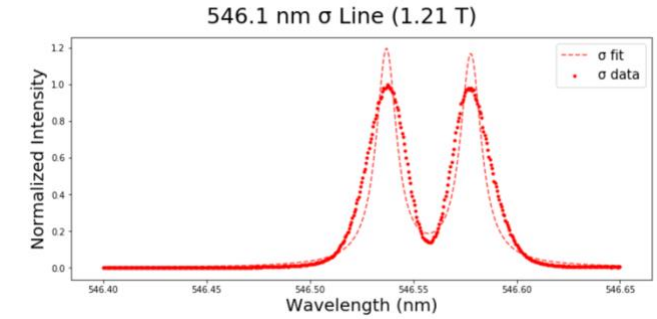

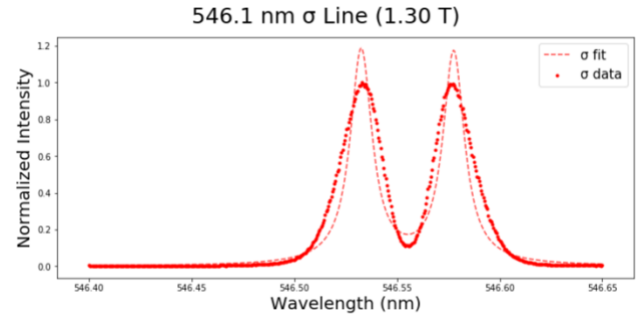

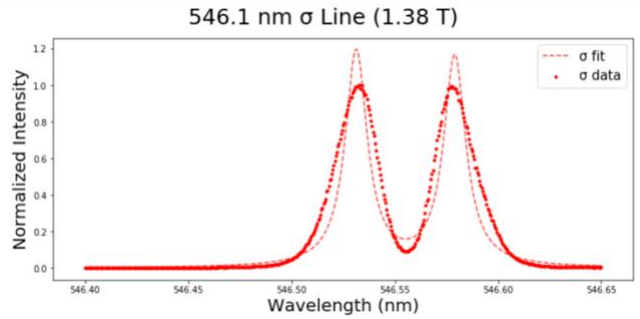

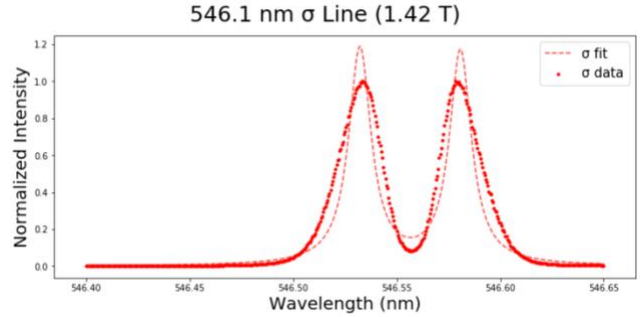

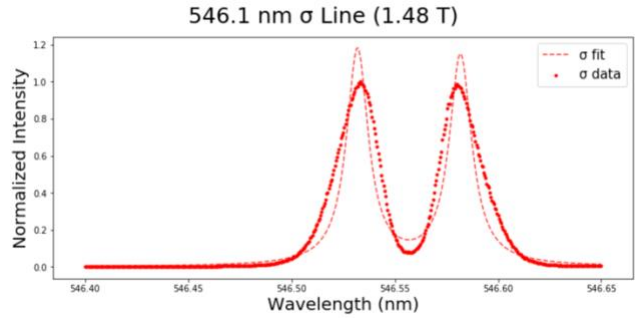

Figure 19 (a-g): Raw data with Lorentzian fits of mercury 546.1 nm σ lines at different magnetic field values

VI.4. Neon $^1S_0 \rightarrow {}^1P_1$ Transition

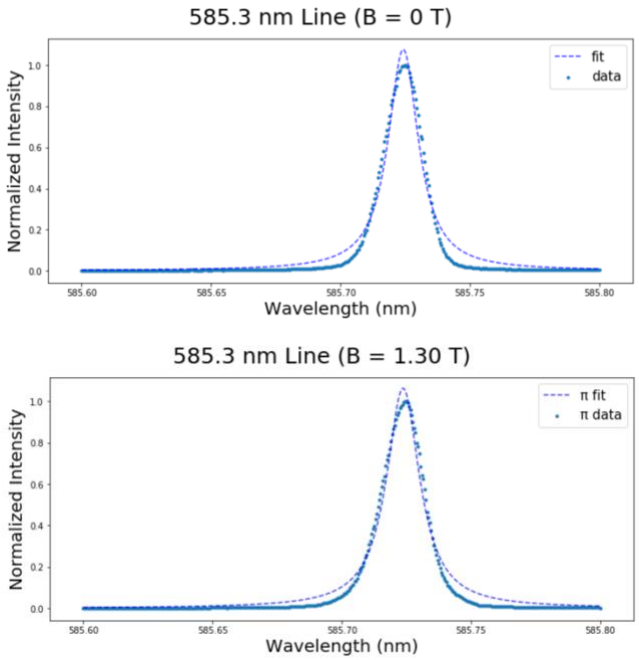

Figure 20 (a-b): Raw data with Lorentzian fit of mercury 585.3 nm π line at different magnetic field values.

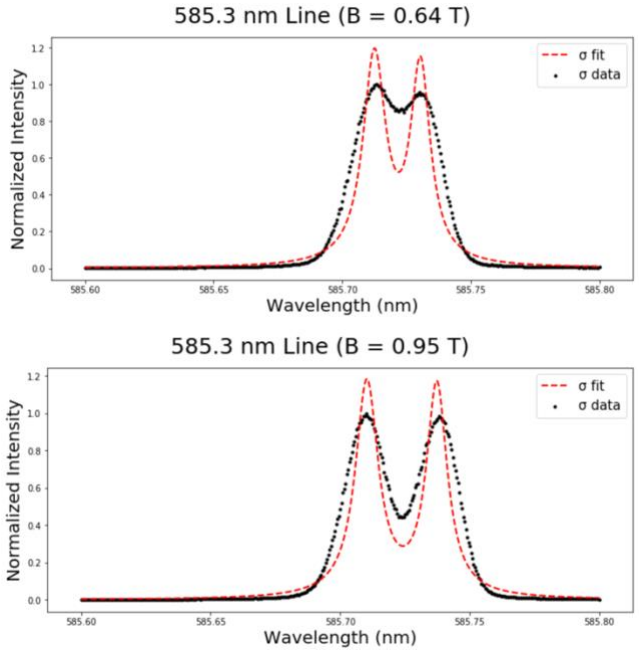

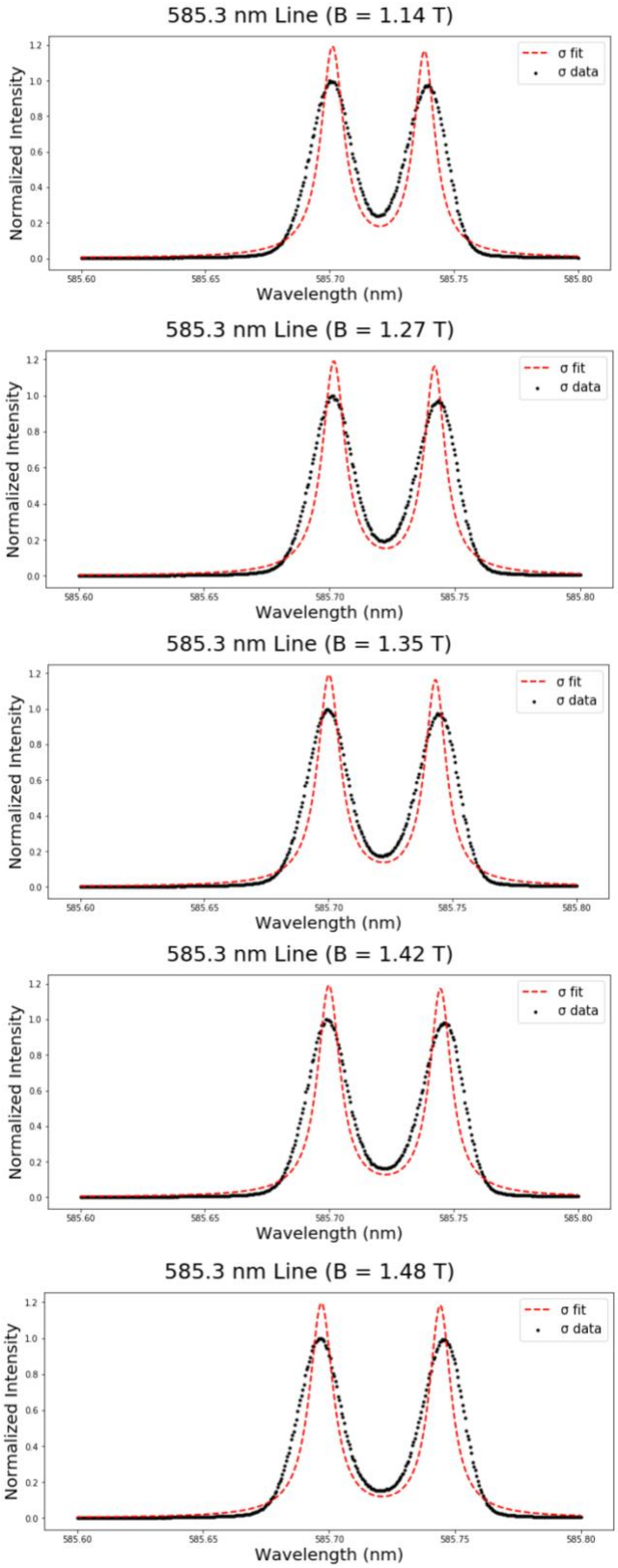

Figure 21 (a-g): Raw data with Lorentzian fits of neon 585.3 nm σ lines at different magnetic field values.